Image Super-Resolution Reconstruction Using Image Registration and Error-Amended Sharp Edge Interpolation

Yung-Yuan CHIEN, Jin-Jang LEOU, and Hsuan-Ying CHEN
Department of Computer Science and Information Engineering
National Chung Cheng University, Chiayi
E-mail: {cyy97m, jjleou, chenhy}@cs.ccu.edu.tw Tel: +886-5-2720411 ext. 33105

***Abstract*—In this study, an image super-resolution (SR) reconstruction approach using image registration and error-amended sharp edge (EASE) interpolation is proposed. The proposed image SR reconstruction approach contains five stages, namely, noise smoothing by Gaussian filtering, image edge map extraction using Canny edge detection, high-resolution grid generation using image registration, EASE interpolation, and blocking artifact reduction by image restoration. Based on the experimental results obtained in this study, both the subjective visual quality and the objective PSNR values of the proposed approach are better than those of the three comparison approaches.**

I. INTRODUCTION

Image super-resolution (SR) reconstruction, an ill-posed problem, is to obtain a high-resolution (HR) image from a single low-resolution (LR) image or multiple LR images having sub-pixel shifts. Image SR reconstruction approaches can be generally classified into three categories, namely, the frequency domain approaches, the spatial domain approaches, and the example-based (learning-based) approaches.

For the frequency domain approaches, for example, Tsai and Huang [1] proposed an image SR reconstruction algorithm, which exploits the shift property of the Fourier transform and developed a set of system equations in the frequency domain that relates the HR image to the observed LR images. Considering only global motion estimation, the performance of frequency domain image SR reconstruction is usually limited by the global motion model.

Several spatial domain approaches [2] were developed to overcome the weaknesses of the frequency domain approaches. Typical spatial domain approaches include non-uniform interpolation, iterative back-projection (IBP), regularization, maximum a posteriori (MAP), projection onto convex sets (POCS), and POCS-embedded MAP. A simple approach to enhance image resolution is non-uniform interpolation, such as bilinear interpolation or cubic interpolation. However, the type of approaches include no additional information for compensating the high-frequency portion of the HR image to be constructed, which has been lost in the LR images. The IBP approach [3] starts with an initial estimate of the SR image, compares the projected LR results with the observed images, and updates the HR estimate based on the predicted errors. The IBP approach is simple, whereas no unique solution to image SR reconstruction can be obtained. Several image SR reconstruction approaches [4-5] used some regularization terms to solve the ill-posed problem. Smoothness priors are usually incorporated as a constraint to reconstruct the HR image. A statistical optimization framework based on a Bayesian estimation theory, namely, MAP, was employed for image SR reconstruction due to its robustness and good performance [6]. The approach makes some simplifications and approximations on probability distribution models to achieve computational tractability. Thus, obtained solutions may violate known SR constraints and all available a priori information may not be completely utilized in the solution process. For the POCS approach [7], prior knowledge about the solution is incorporated into the SR reconstruction procedure. The POCS approach restricts the solution to be one among a closed convex set that satisfies a particular property, and then the final solution will be in the intersection of all constrained sets. For the POCS-embedded MAP image SR reconstruction approach [8], both the Bayesian theory and the convex set theoretic technique are used to get the better SR image(s).

For example-based SR reconstruction, correspondences between HR and LR image patches are learned from a database, which are applied to each LR image to recover its most likely HR version. Most example-based SR approaches [9-10] involved a training set containing a large number of HR image patches and their corresponding LR image patches. That is, most learning-based SR reconstruction approaches treat the "learning" process as just a kind of "searching" the best-matched LR image patch, and then "pasting" the corresponding HR image patch.

In this study, an image super-resolution (SR) reconstruction approach using image registration and error-amended sharp edge (EASE) interpolation is proposed. The proposed image SR reconstruction approach contains five stages, namely, noise smoothing by Gaussian filtering, image edge map extraction using Canny edge detection, high-resolution grid generation using image registration, EASE interpolation, and blocking artifact reduction by image restoration.

II. THE OBSERVATION MODEL

An observation model describing the relationship between HR and LR images for image SR reconstruction is shown in Fig. 1 [11]. If **x** denotes an HR image that is sampled from the original continuous scene. Then, the *f*-th observed LR image $\mathbf{y}_f$, processed by the warping ($\mathbf{M}_f$), blurring ($\mathbf{B}_f$), and downsampling (**D**) operators and additive noise ($\mathbf{n}_f$), can be obtained as

$$\mathbf{y}_f = \mathbf{D}\mathbf{B}_f\mathbf{M}_f\mathbf{x} + \mathbf{n}_f. \quad (1)$$

III. Proposed Approach

Exiting image SR reconstruction approaches often have some noise and blurring related problems, particularly in edge regions. The proposed approach will deal with the noise and blurring related problems in edge regions. Most image SR reconstruction approaches usually contains three main steps, namely, registration, interpolation, and restoration. As shown in Fig. 2, two extra stages are included in the proposed image SR reconstruction approach. One is the pre-processing stage used to perform noise removal and restore the LR images. Another is edge detection performed on the reference LR image to extract its edge map.

A. Pre-Processing

The LR images acquired by an imaging sensor are usually affected (blurred) by the point spread function (PSF) of the imaging sensor and noise. Here, a pre-processing step will be performed on the blurred LR images. As shown in Fig. 3, given an original HR image *x*, and some knowledge about the degradation function ***C*** and the additiive Gaussian noise ***n***, the objective is to obtain an estimate $\hat{y}$ of the LR image *y*.

To reduce the additive Gaussian noise, the 2D Gaussian filter is used, which can be described as

$$G(x,y) = \frac{1}{\sqrt{2\pi}\sigma} e^{-(x^2+y^2)/2\sigma^2}, \quad (2)$$

where σ is the standard deviation of the 2D Gaussian filter. The Gaussian filter, a type of low-pass filter, will attenuate the high frequency parts of an image and can be realized by convoluting a filtering mask. To keep more edge information, either a 5×5 or a 7×7 filtering mask is used in this study.

B. Canny Edge Detection

In this study, a reference image, denoted $\hat{y}_{\text{ref}}$, will be selected from the LR images. The reference image $\hat{y}_{\text{ref}}$ will perform Canny edge detection, which contains the following steps: i) smooth the image by the Gaussian filter, ii) compute the image gradients (magnitudes and orientations) by the finite-differences of the first-order derivative, iii) restrain the non-maximum value of the gradient's magnitude, iv) detect and connect the image's edges by hysteresis thresholding.

First, a Gaussian filter is used to remove noise. For example, a 5×5 discrete approximation of the 2D Gaussian filter with σ =1.4 can be described as

$$I = \frac{1}{115}\begin{bmatrix} 2 & 4 & 5 & 4 & 2 \\ 4 & 9 & 12 & 9 & 4 \\ 5 & 12 & 15 & 12 & 5 \\ 4 & 9 & 12 & 9 & 4 \\ 2 & 4 & 5 & 4 & 2 \end{bmatrix}. \quad (3)$$

After noise reduction, 2-D signal gradient filters are adopted to extract edges in vertical, horizontal, and two diagonal directions. Based on S_x and S_y obtained by the Sobel operators for vertical and horizontal edge detections, the gradient strength (magnitude), *S*, is approximated by

$$|S| = |S_x| + |S_y|. \quad (4)$$

The edge direction is defined as

$$\theta = \tan^{-1}\left(\frac{S_y}{S_x}\right). \quad (5)$$

Here, edge directions within (0°, 22.5°) and (157.5°, 180°) are rounded to 0°, edge directions within (22.5°, 67.5°) are rounded to 45°, edge directions within (112.5°, 157.5°) are round to 135°, and edge directions within (67.5°, 112.5°) are rounded to 90°. For the special case S_x=0, edge direction θ is set to either 0° or 90°.

After edge directions are determined, non-maximum suppression is then applied, which is used to trace each edge along its direction and suppress any pixel (set its value to 0) that dose not belong to any edge. This will result in thin edges in the output image.

Afterwards, Canny edge detection performs hysteresis thresholding with a low threshold and a high threshold. Edge pixels stronger than the high threshold are marked as "strong," edge pixels weaker than the low threshold are suppressed, and edge pixels between the two thresholds are marked as "weak." Hysteresis thresholding can avoid false edge pixels. Starting with the high threshold and the early-extracted directions, edges can be well traced. Finally, a binary image, namely, the reference edge map $\boldsymbol{e}_{\text{ref}}$, is extracted to reconstruct the desired HR image in the next stage.

C. Image Registration

As shown in Fig. 2, after pre-processing, the reference LR image, $\hat{y}_{\text{ref}}$, will be processed by Canny edge detection and image registration simultaneously. In the image registration stage, first, the reference LR image will be interpolated by linear interpolation with magnification factor $MF = 2 \times 2$ and the interpolated reference image is divided into four equal-sized sampled images. The relationship between the reference LR image and the four equal-sized sampled images is illustrated in Fig. 4. The pixels marked as "1" in the reference image and the first sampled image are important pixels, which will not be modified. The pixels in the other three sampled images marked as "2," "3," and "4," are obtained by image interpolation, which are relatively unreliable. To improve their reliability, the pixel values of the three other sampled

images marked as "2," "3," and "4," in the interpolated image (Fig. 4(b)) might be replaced by the pixel values of other "original" LR images, whereas the pixels marked by "1" in the interpolated image (i.e., the pixels of the original reference LR image) are not modified. The mean square error (MSE) is used for comparing the pixels in the other original LR images with the pixels marked as "2," "3," and "4," in the interpolated image and then the pixel (from some other LR image) having the minimum MSE value is selected to replace the corresponding pixel (marked as "2," "3," or "4," in the interpolated image). Note that all the pixels in the interpolated reference image are re-determined, as an illustrated example shown in Fig. 5(a). However, the re-determined reference image, called the registered image, is not always so good. For example, the smallest pixel value may have a large gap, resulting in a poor result. Here, for the gaps larger than the threshold P, the corresponding pixel values of the interpolated image will be replaced by those from the original reference LR image rather than those from other LR images, as an illustrated example shown in Fig. 5(b).

Sometimes, some pixel values of the interpolated image are not always re-determined (such as the pixels marked as "?" in Fig. 5(c)). Here, the Euclidean distances between a pixel marked as "?" and its neighboring grid pixels in the interpolated image are computed, and the three nearest pixels around the pixel marked as "?" are detected. The pixel value of the pixel marked as "?" is finally re-determined as the weighted average pixel value of the three nearest pixels. Then, we obtain the registered HR image.

To address the image registration stage, Figs. 4 and 5 show an illustrated example with $MF = 2 \times 2$. For the illustrated example with $MF = 3 \times 3$, nine sampled images will be generated. Other cases can be similarly processed.

D. Error-Amended Sharp Edge (EASE) Interpolation

The registered HR image can be decomposed into two parts: smooth regions and edge regions. In a smooth region, because the pixels contain small variations, the registration stage will result in good HR image results, whereas in an edge region, there are serious block artifacts. Therefore, in the next stage, EASE interpolation will be applied on the registered HR image, based on its reference edge map.

To remove/reduce image artifacts, such as the checkerboard effect in the registered image, EASE interpolation [12], a modified version of bilinear interpolation, is used. Based on the reference edge map, $\boldsymbol{e}_{\text{ref}}$, of the reference LR image, EASE interpolation is used to remove/reduce image artifacts in the edge regions. In fact, the reference edge map, $\boldsymbol{e}_{\text{ref}}$, will be enlarged with the same MF of the interpolated reference image. Then, the enlarged reference edge map is used to improve the edge regions of the registered HR image by EASE interpolation [12].

E. Image Restoration

By use of image registration and nonuniform EASE interpolation, the obtained HR image still contains some blocking artifacts. Here, the technique proposed by Vinh and Kim [13] is used to further reduce some block artifacts. The technique classifies all the pixels into two classes: smooth regions and edge regions. An adaptive offset smoothing scheme is used to reduce grid noises on block boundaries and an extra edge-preserved filter is used to remove block artifacts in edge regions. After further block artifact reduction, the final HR image is obtained.

IV. Experimental Results

The proposed image SR reconstruction approach has been implemented on an Intel Core 2 6300 1.86 GHz PC with 4GB main memory using Borland C++ Builder 6 software develop tool. To evaluate the performance of the proposed approach, three comparison image SR reconstruction approaches are implemented in this study, including (1) the IBP-based approach proposed by Dai et al. [3], (2) a joint registration and image SR image reconstruction approach by Vandewalle et al. [4], and (3) a learning-based image SR reconstruction approach proposed by Kim and Kwon [10]. In this study, four test images, "Peppers," "House," "Lena," and "Baboon," are used to evaluate the performances of the three comparison approaches and the proposed approach. The four images are 512×512 in size. In the observation model, the original HR images are blurred using a $k \times k$ uniform mask, and decimated using the down-sampling factor $l \times l$. Three different down-sampling factors (2×2, 3×3, and 4×4) are employed in the study. Finally, the additive zero-mean white Gaussian noise (AWGN) with standard deviation σ_n is added and the simulated LR images are thus obtained.

To obtain accurate reference edge maps, the low and high thresholds for hysteresis thresholding must be well set. The low and high thresholds of the four test images for hysteresis thresholding are listed in Table I. The image SR reconstruction results of "Peppers" with k=8, l=2, and σ_n=10 by the three comparison approaches and the proposed approach are shown in Fig. 6. The image SR reconstruction results of "House" with k=3, l=2, and σ_n=8 by the three comparison approaches and the proposed approach are shown in Fig. 7. The image SR reconstruction results of "Lena" with k=4, l=3, and σ_n=7 by the three comparison approaches and the proposed approach are shown in Fig. 8. The image SR reconstruction results of "Baboon" with k=5, l=4, and σ_n=6 by the three comparison approaches and the proposed approach are shown in Fig. 9. In terms of PSNR (peak-signal-to-noise-ratio) in dB, the performance comparisons between the three comparison approaches and the proposed approach for the four test images shown in Figs. 6-9 are listed in Table II. Based on the experimental results shown in Figs. 6-9 and Table II, both the visual quality and PSNR values of the proposed approach are better than those of the three comparison approaches.

V. Concluding Remarks

In this study, an image super-resolution (SR) reconstruction approach using image registration and error-amended sharp edge (EASE) interpolation is proposed. The proposed image

SR reconstruction approach contains five stages, namely, noise smoothing by Gaussian filtering, image edge map extraction using Canny edge detection, high-resolution grid generation using image registration, EASE interpolation, and blocking artifact reduction by image restoration. Based on the experimental results obtained in this study, both the subjective visual quality and the objective PSNR values of the proposed approach are better than those of the three comparison approaches.

ACKNOWLEDGEMENTS

This work was supported in part by National Science Council, Taiwan, Republic of China under Grants NSC 98-2221-E-194-034-MY3 and NSC 99-2221-E-194-032-MY3.

REFERENCES

[1] R. Y. Tsai and T. S. Huang, "Multi-frame image restoration and registration," *Advances in Computer Vision and Image Process.*, vol. 1, pp. 317-339, 1984.

[2] C. Papathanassiou and M. Petrou, "Super resolution: an overview," in *Proc. of 2005 IEEE Int. on Geoscience and Remote Sensing Symposium*, vol. 8, 2005, pp. 5655-5658.

[3] S. Y. Dai, M. Han, Y. Wu, and Y. H. Gong, "Bilateral back-projection for single image super resolution," in *Proc. of IEEE Int. Conf. on Multimedia and Expo*, 2007, pp. 1039-1042.

[4] P. Vandewalle, L. Sbaiz, J. Vandewalle, and M. Vetterli, "Super-resolution from unregistered and totally aliased signals using subspace methods," *IEEE Trans. on Signal Process.*, vol. 55, no. 7, pp. 3687-3703, 2007.

[5] S. Y. Dai, M. Han, W. Xu, Y. Wu, Y. Gong, and A. K. Katsaggelos, "Softcuts: a soft edge smoothness prior for color image super-resolution," *IEEE Trans. on Image Process.*, vol. 18, no. 5, pp. 969-981, 2009.

[6] J. Tian and K. K. Ma, "Stochastic super-resolution image reconstruction," *Journal of Visual Communication and Image Representation*, vol. 21, no. 3, pp. 232-244, 2010.

[7] M. Gevrekci, B. K. Gunturk, and Y. Altunbasak, "POCS-based restoration of Bayer-sampled image sequences," in *Proc. of IEEE Int. Conf. on Acoustics, Speech and Signal Process.*, vol. 1, 2007, pp. 753-756.

[8] B. G. Wei and W. H. Hui, "POCS-embedded MAP method for image super-resolution restoration," in *Proc. of IEEE Conf. on Industrial Electronics and Applications*, 2009, pp. 3791-3794.

[9] D. Glasner, S. Bagon, and M. Irani, "Super-resolution from a single image," in *Proc. of 2009 IEEE Int. Conf. on Computer Vision*, 2009, pp. 349-356.

[10] K. I. Kim and Y. Kwon, "Single-image super-resolution using sparse regression and natural image prior," *IEEE Trans. on Pattern Analysis and Machine Intelligence*, vol. 32, no. 6, pp. 1127-1133, 2010.

[11] S. Park, M. Park, and M. G. Kang, "Super-resolution image reconstruction: a technical overview," *IEEE Signal Process. Mag.*, vol. 20, no. 5, pp. 21-36, 2003.

[12] Y. Cha and S. Kim, "The error-amended sharp edge (EASE) scheme for image zooming," *IEEE Trans. on Image Process.*, vol. 16, no. 6, pp. 1496-1505, 2007.

[13] T. Q. Vinh and Y. C. Kim, "Block artifact reduction based on pixel classification using binary edge map," in *Proc. of Int. Conf. on Advanced Language Process. and Web Information Technology*, vol. 1, 2008, pp. 193-197.

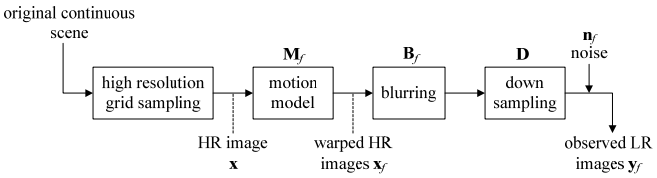

Fig. 1. Observation model for image SR reconstruction [11].

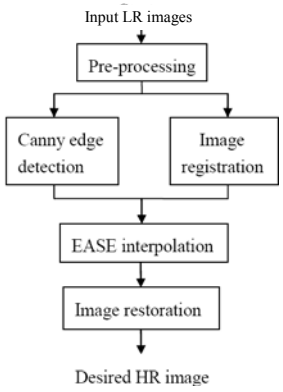

Fig. 2. The framework of the proposed image SR reconstruction approach.

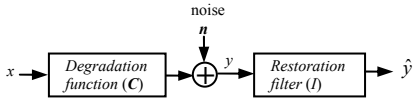

Fig. 3. A model of the image degradation/restoration process.

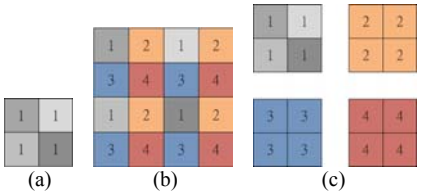

Fig. 4. (a) The reference LR image; (b) the interpolated image by bilinear interpolation with MF=2×2; (c) the four corresponding sampled images.

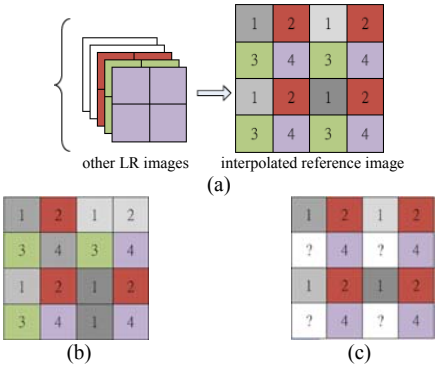

Fig. 5. (a) The pixels in the other LR images can be used to re-determine the pixels marked as "2," "3," and "4," in the interpolated image; (b) the case that some pixel value is replaced by the pixel value from the original LR image; (c) the case that some pixels are marked as "?."

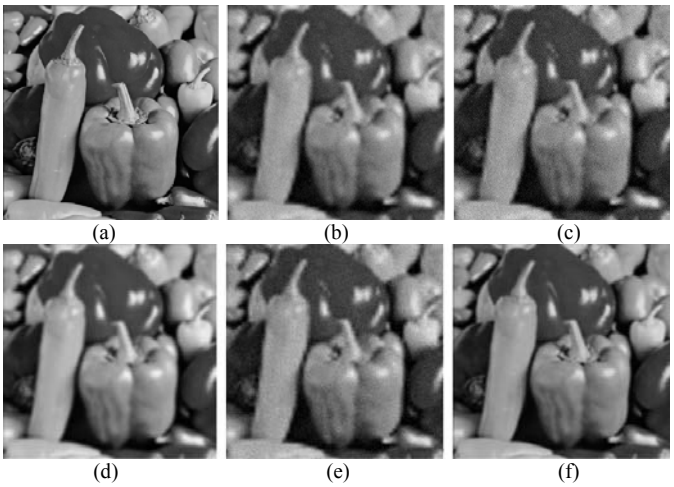

Fig. 6. The image SR reconstruction results of "Peppers" with k=8, l=2, and σ_n=10: (a) the original image; (b) the interpolated LR image; (c)-(f) the image SR reconstruction results by the IBP-based approach [3], the rank-based approach [4], the learning-based approach [10], and the proposed approach, respectively.

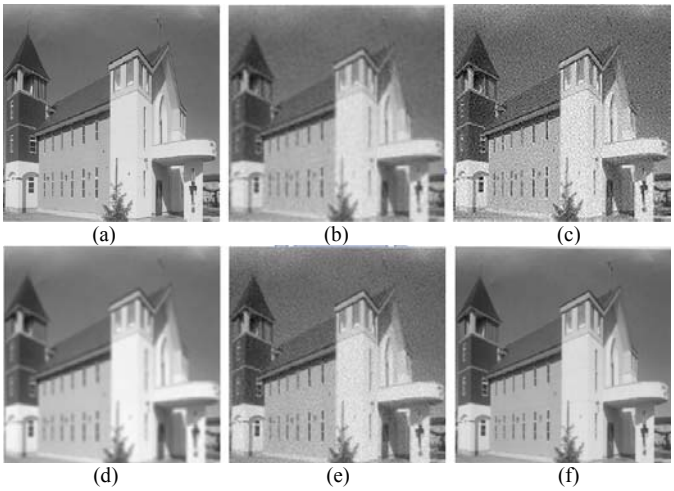

Fig. 7. The image SR reconstruction results of "House" with k=3, l=2, and σ_n=8: (a) the original image; (b) the interpolated LR image; (c)-(f) the image SR reconstruction results by the IBP-based approach [3], the rank-based approach [4], the learning-based approach [10], and the proposed approach, respectively.

Fig. 8. The image SR reconstruction results of "Lena" with k=4, l=3, and σ_n=7: (a) the original image; (b) the interpolated LR image; (c)-(f) the image SR reconstruction results by the IBP-based approach [3], the rank-based approach [4], the learning-based approach [10], and the proposed approach, respectively.

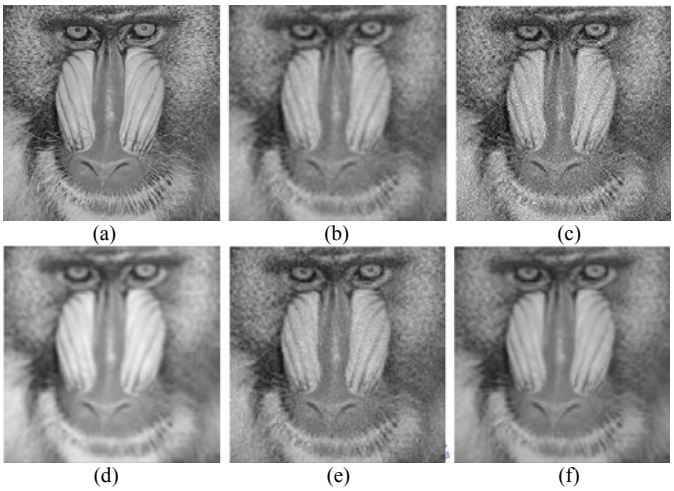

Fig. 9. The image SR reconstruction results of "Baboon" with k=5, l=4, and σ_n=6: (a) the original image; (b) the interpolated LR image; (c)-(f) the image SR reconstruction results by the IBP-based approach [3], the rank-based approach [4], the learning-based approach [10], and the proposed approach, respectively.

TABLE I

THE LOW AND HIGH THRESHOLDS OF THE FOUR TEST IMAGES FOR HYSTERESIS THRESHOLDING.

	Low threshold	High threshold
Peppers	0.037	0.093
House	0.078	0.197
Lena	0.050	0.125
Baboon	0.161	0.397

TABLE I I

IN TERMS OF PSNR IN DB, THE PERFORMANCE COMPARISONS BETWEEN THE THREE COMPARISON APPROACHES AND THE PROPOSED APPROACH FOR THE FOUR TEST IMAGES SHOWN IN FIGS. 6-9.

	IBP-based [3]	Rank-based [4]	Learning-based [10]	Proposed
Peppers	19.94	22.88	21.28	26.05
House	20.73	20.62	21.28	25.20
Lena	22.17	23.03	23.48	26.99
Baboon	17.70	16.71	19.28	19.82